



# Novel adsorbents for simultaneous extraction of lead and cadmium ions from polluted water: based on active carbon, nanometal (Zr-Ce-Sm)-mixed oxides and iron-alginate beads

Sneha Latha Pala<sup>1</sup> · Suneetha Mekala<sup>2</sup> · Kunta Ravindhranath<sup>1</sup>

Received: 15 May 2022 / Revised: 7 July 2022 / Accepted: 9 July 2022 / Published online: 22 July 2022  
© The Author(s), under exclusive licence to Springer-Verlag GmbH Germany, part of Springer Nature 2022

## Abstract

Nanoparticles of mixed n(Zr-Ce-Sm) oxide of crystalline size 11.7 nm are successfully synthesized by new green methods adopting *Aloe vera* gel as capping agent and evoking the principles of classical methods of homogenous precipitations. An active carbon is derived from stems of *Artocarpus heterophyllus* plant. The *Artocarpus heterophyllus* active carbon (AHAC), active carbon loaded with nanoparticles 'AHAC + n(Zr-Ce-Sm) oxide' and iron alginate beads doped with their admixture, 'AHAC + n(Zr-Ce-Sm) oxide-Fe.Ali', are investigated for their effectiveness for the simultaneous removal of lead and cadmium ions from water. Different extraction conditions are optimized for the maximum efficiency of the three sorbents by batch methods. The sorbents have shown good sorption nature for both the toxic ions at the pHs: 6.0 for active carbon, 6.5 for admixture and 7.0 for beads respectively at different equilibration times and dosages. The maximum adsorption capacities for Pb<sup>2+</sup>/Cd<sup>2+</sup> ions are as follows: 15.0/20.0, 28.0/32.6, 34.0/44.3 mg/g for AHAC, admixture and beads respectively. The sorbents are characterized for various physicochemical parameters and structural aspects using XRD, FTIR, EDX and FESEM. The effects of co-ions on the simultaneous extraction are investigated. The mechanism of the adsorption process is analysed based on thermodynamic data and applicability of isotherms and kinetic models. Based on these, the mechanism of adsorption process involves the formation of a surface complex and/or ion-exchange between Pb<sup>2+</sup>/Cd<sup>2+</sup> with the surface functional groups of adsorbents. The same is confirmed by IR investigations. The spent adsorbents can be regenerated and reused. The adsorbents developed are successfully used to treat the industrial waste water samples. The merit of this investigation is that the effective sorbents with high adsorption capacities are developed for the simultaneous remove of the highly toxic lead and cadmium ions from industrial wastewater.

**Keywords** Simultaneous removal · Lead and cadmium ions · Adsorption · *Artocarpus heterophyllus* · *Aloe vera* gel · Thermodynamic · Kinetic and isothermal studies · Applications

## 1 Introduction

The contamination of natural water with heavy metal ions is one of the major threats to the environment [8, 23]. The basic source of contamination is the improperly treated discharges of industrial wastes into the environments [24,

32]. Lead and cadmium ions are the prominent heavy metal ions present in the discharges from industries based on mining, paints, batteries, ceramics, galvanization, electro-plating, petrochemicals, lead piping and metallurgical etc. [8, 32]. The said heavy metal ions once enter into the water bodies, their concentration is amplified with times as they are non-degradable and involve in many metabolic processes of organisms and plants. These ions are highly toxic even at low concentrations and are considered as carcinogenic heavy metals [32, 48]. As per WHO [64, 65] recommendations, the permissible limits of lead and cadmium are 0.01 mg/L and 0.003 mg/L respectively. Hence, it is very essential that lead and cadmium should be removed from contaminated water before discharging into water bodies [64, 65].

✉ Kunta Ravindhranath  
ravindhranath.kunta@gmail.com

<sup>1</sup> Department of Chemistry, Koneru Lakshmaiah Education Foundation, Green Fields, Vaddeswaram-522 502, Guntur Dt., Vaddeswaram, Andhra Pradesh, India

<sup>2</sup> Department of Chemistry, RGUKT-Nuzvid, Nuzividu, Andhra Pradesh, India

As such, intensive research throughout the globe is being pursued in finding cost-effective methods to remove these toxic contaminants from wastewater. Several methods such as membrane separation, ion exchange, chemical precipitation, electro-kinetics, adsorption, electroplating and chemical coagulation are employed for the removal of toxic lead and cadmium ions from polluted water [26, 37]. Among them, the adsorption processes are considered to be low-cost, simple, efficient and easily adoptable technique owing to the availability of various adsorbents with high metal binding capacities [13, 57]. In recent years, more attention is devoted in using the plant materials or their derivatives as bio-sorbents for the removal of toxic pollutants from waste water because of their easy availability, eco-friendliness, cost-effectiveness and renewable nature [13, 19, 29, 30, 33, 47, 51, 54, 56–60]. But one of the major disadvantages of these bio-sorbents is their low adsorption capacities. To increase the capacity, the bio-sorbents are loaded with nanoparticles. The nanoparticles due to their large surface area and other physicochemical properties inherited due to the nano-size enhance the sorption nature of active carbons. The main hurdle of these mixed materials using as adsorbents is that the nanomaterials undergo ‘agglomeration’ and filtration is slow. To get rid of these limitations, the material is to be doped into beads or plastic materials [12, 14, 50, 52, 53].

In the present investigation, various adsorbents were investigated for their affinity for lead and cadmium ions and identified that the active carbon synthesized from the stems of *Artocarpus heterophyllus* plant was effective. Furthermore, nanoparticles of (Zr-Ce-Sm) oxide were successfully synthesized using new green routes adopting *Aloe vera* gel extract as ‘capping or stabilizing agent’ and evoking the principles of homogenous methods of precipitation in preventing growth of the particle beyond nano-size. These nanoparticles were admixed with the active carbon and the resulting blend was doped in iron-alginate beads with an aim to have the cumulative benefits of the porous nature of active carbon, surface properties of nanoparticles and sorption nature of iron-alginate beads towards the lead and cadmium ions. Thus the active carbon, nanoparticle-loaded active carbon and the beads were investigated for their effectiveness for the removal of lead and cadmium ions from polluted water.

## 2 Materials and methods

### 2.1 Chemicals and solution

All chemicals and reagents used in this work were of analytical grade and purchased from Merck, India Pvt. Ltd.

and S.D. Chemicals, India. Simulated stock solutions of lead and cadmium ions of concentrations 20.0 mg/L and 15.0 mg/L respectively were employed in this investigation. The solutions and reagents were prepared as described in the literature [9].

### 2.2 Syntheses of adsorbents

Various bio-materials pertaining to different species of plants were investigated for their adsorptivity for lead and cadmium ions. It was observed that the active carbon generated from the stems of *Artocarpus heterophyllus* plant had shown marked affinity towards both the lead and cadmium ions. Hence, the said active carbon was investigated.

#### 2.2.1 Preparation of active carbon

The stem pieces of *Artocarpus heterophyllus* plant were washed with distilled water, half-dried treated with sufficient conc.  $\text{H}_2\text{SO}_4$  in a round bottom flask of sufficient capacity and kept aside for overnight. Then the material in the round bottom flask was heated under water condenser set-up (after further addition of conc.  $\text{H}_2\text{SO}_4$  if needed) until the material was completely carbonized. Thus carbonized material was filtered, washed for neutrality, dried at 105 °C, cooled and preserved in a brown bottle. The active-carbon obtained from the stems of *Artocarpus heterophyllus* plant was termed as AHAC.

#### 2.2.2 Synthesis of composite, ‘AHAC + n(Zr-Ce-Sm) oxide’

To improve the sorption nature of AHAC, various nanoparticles of  $\text{ZrO}_2$ ,  $\text{CeO}_2$  and  $\text{Sm}_2\text{O}_3$  and their combinations were loaded onto AHAC and noted that the ternary nanometal (Zr-Ce-Sm) oxide was found to be effective. We found a new green route for the synthesis of the said mixed nanometal oxide and it was described hereunder.

**Synthesis of ‘nano (Zr-Ce-Sm)-oxide’ Capping agent:** Of various plant extracts investigated, *Aloe vera* gel extract was found to be effective. The gel was scrapped from the folded leaves of the plant. The collected material was crushed and subjected to intensive stirring for obtaining a nearly homogeneous solution. The solution was centrifuged at 10,000 rpm and the filtrate was stored at 5.0 °C. This extract was effective as a capping and stabilizing agent in the formation of nano-mixed metal oxide.

**Synthesis of nano-mixed metal oxides:** A total of 2.0 g of  $\text{ZrOCl}_2 \cdot 8\text{H}_2\text{O}$ , 1.5 g of  $(\text{NH}_4)_2\text{Ce}(\text{NO}_3)_6$  and 1.0 g of  $\text{Sm}_2\text{O}_3$  were added to 100.0 mL 1:1 HCl taken in a 250-mL beaker. The solution was heated to 75 °C with constant

stirring to get a clear solution. To the resulting solution, needed amount of ethylene glycol was added to make the solution 10% with respect to ethylene glycol content. Then, 5.0 g of *Aloe vera* gel extract and 5.0 g of urea were added. The resulting solution was heated to raise the temperature slowly while constantly stirring the solution. The urea got hydrolysed to generate ammonia (precipitant), which in turn increased the pH of the solution. The slow generating of the precipitating agent, NH<sub>3</sub> and more viscosity of the mother liquor prevent the conditions of super saturation at local points of precipitation and thereby resulting in the slow ‘nucleation’ of the hydroxides of Zr, Ce and Sm. The mixed oxides when they reached the nano-size, the capping agent, *Aloe vera* gel extract, seems to prevent the further growth by ‘capping’ the surface of the particles.

The heating of the solution was continued until pH of the solution had reached to pH: 9.0. The subjective heating was stopped but stirring continued for 3.0 h. The solution was centrifuged for nanoparticles, thoroughly washed with distilled water and dried. The material was calcinated using muffle furnace for 5.0 h at the temperature: at 550 °C. The nanoparticles of ‘n(Zr-Ce-Sm) oxide’ were preserved in air-tight brown-bottle.

**Embedding nanoparticles in the matrix of the active carbon** Successively, 1.0 g of (Zr-Ce-Sm) oxide and 4.0 g of AHAC were added to 100 mL of distilled water in a beaker. Then, the solution was heated at 60 °C for 3.0 h with constant stirring. The obtained material was centrifuged and particles were washed with distilled water. Then, the composite was dried at 110 °C for 3.0 h. The obtained n(Zr-Ce-Sm) oxide-loaded AHAC was named as ‘AHAC + n(Zr-Ce-Sm) oxide’.

### 2.2.3 Iron alginate beads doped with active carbon and nanoparticles ‘AHAC + n(Zr-Ce-Sm)oxide-Fe.Ali’

A total of 100 mL of distilled water was taken in a 250-mL beaker. To this, 2.5 g of sodium alginate was added and heated to 70 °C with constant stirring until a gel-like solution was obtained. Then, 2.5 g of ‘AHAC + n(Zr-Ce-Sm) oxide’ was added and stirred until to get a homogeneous solution. After cooling, this solution was added in drop-wise into a previously cooled (10 °C) 3.0% ferric chloride solution. Beads embedded with ‘AHAC + n(Zr-Ce-Sm) oxide’ were formed. These beads were digested with its mother liquor for overnight, filtered, washed and dried at 80 °C for 2.0 h. Thus, synthesized beads were named as ‘AHAC + n(Zr-Ce-Sm) oxide-Fe.Ali’ beads. The various stages of preparation of adsorbents are summarized in the Fig. 1.

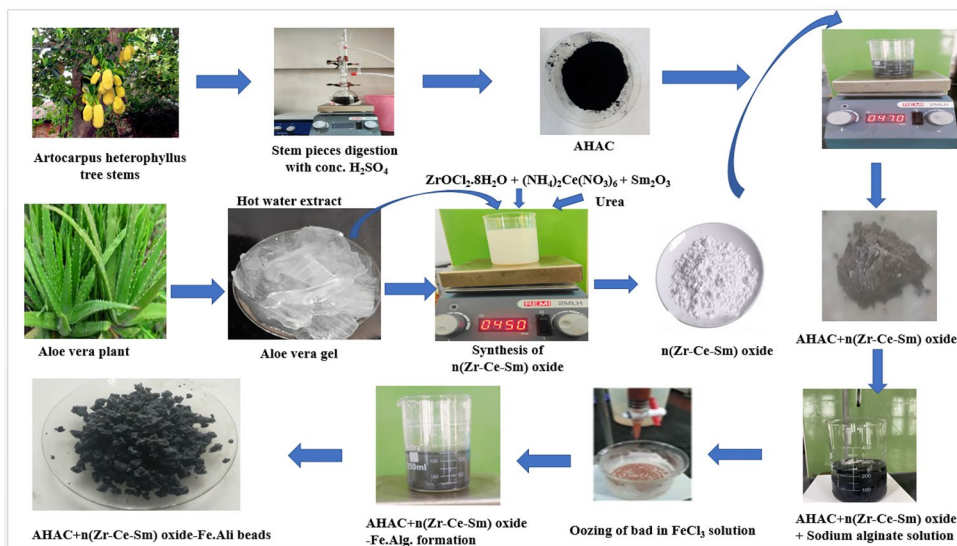
### 2.3 Characterizations

Various physicochemical parameters such as ash (%) [44], moisture (%) [16], iodine number (mg/g) [10], particle size (μ) [22], apparent density (g/mL) [16] and BET-surface area (m<sup>2</sup>/g) [15] of the developed adsorbents in this study were characterized as per the standard procedures in the literature. The results are presented in the Table 1.

Furthermore, ‘before and after’ adsorption of lead and cadmium ions, the surface morphology of the adsorbents was characterized by adopting X-ray diffraction (XRD), Fourier transform infrared (FTIR) spectroscopy, field emission scanning electron microscopic (FESEM) and energy-dispersive X-ray spectroscopy (EDX) techniques.

XRD patterns of the adsorbents were measured by using PAN analytical X-ray diffract metre using Cu Kα source at 1.54 Å. BRUKER ALFA FTIR spectrophotometer (KBr pellet method) was used to note FTIR spectra in the range 4000–500 cm<sup>-1</sup>. FESEM images and EDX spectra were

Fig. 1 Graphical presentation of synthesis of various adsorbents



noted using the instrument FESEM, Zeiss, Sigma, Germany, equipped with FESEMEDX at the optimum voltage of 3.0 kV with ultra-high resolution. The results obtained are presented in Figs. 2, 3, 4 and 5.

## 2.4 Batch adsorption experiments

Batch mode of experiments was conducted for the removal of lead and cadmium ions from water by using AHAC, ‘AHAC + n(Zr-Ce-Sm) oxide’ and ‘AHAC + n(Zr-Ce-Sm) oxide-Fe.Ali’ beads as adsorbents. The experiments were performed in 250-mL stoppered flasks which contain 100 mL each of Pb<sup>2+</sup> (20 mg/L) and/or Cd<sup>2+</sup> (15 mg/L) solutions. Measured quantities of the adsorbents were added and the initial pH of the solutions was adjusted within the range of 2–12 using dil. HCl/dil. NaOH. Then, stoppered flasks were shaken in an orbital-shaker at 350 rpm at the room temp.: 30 ± 1 °C for a given agitation time and then, the solutions were filtered. The AAS method (240AASF, Agilent, USA) was adopted for the determination of un-extracted amounts of Pb<sup>2+</sup> or Cd<sup>2+</sup> in the filtrate as described in the literature [51–53]. Using the following equations adsorption capacity and percentage removal was assessed.

$$\text{Adsorption capacity} : (q_e) = \frac{(C_i - C_e)V}{m}$$

$$\% \text{removal} (\%R) = \frac{(C_i - C_e)}{C_i} \times 100$$

where  $C_i$  is the initial Pb<sup>2+</sup>/Cd<sup>2+</sup> concentration,  $C_e$  is the equilibrium Pb<sup>2+</sup>/Cd<sup>2+</sup> concentration, and  $V$  is the simulated

solution volume (L);  $m$  is the sorbent mass (g) which were evaluated.

In these investigations, the effect of various experimental conditions on lead and cadmium removal was assessed by varying pH, 2–12; agitation time, 15–150 min; adsorbent dosage, 0.25 to 3.0 g/L; initial metal ion concentrations, 5–50 mg/L; and temperature, 303–333 K. During this study, the targeted parameter only varied progressively and all other extraction conditions were maintained at fixed optimum values. The effect of co-ions was also investigated. Regeneration studies on the spent adsorbents were performed with various eluents.

The results of adsorption experiments were described and analysed by four isotherm models: Freundlich, Langmuir, Dubinin-Radushkevich (D-R) and Temkin; and four kinetic models: pseudo first-order, pseudo second-order, Bhangam’s pore diffusion and Elovich. The adsorption nature was analysed thermodynamically. The developed methodology was used to treat real polluted water samples collected from the effluents of industries. Findings are presented in Figs. 6, 7, 8, 9, 10 and 11 and Tables 2, 3, 4, 5, 6 and 7.

## 3 Results and discussions

### 3.1 Characterization studies

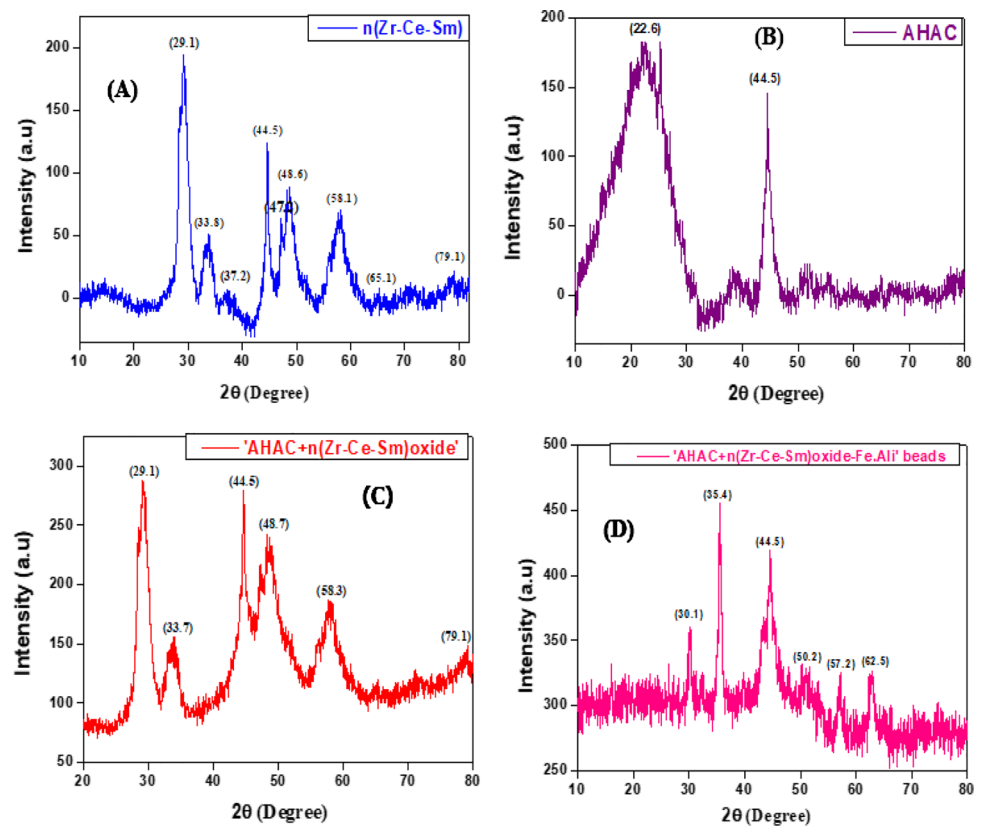
#### 3.1.1 Physicochemical parameters

The physicochemical parameters of the adsorbents, AHAC, AHAC + n(Zr-Ce-Sm) oxide and

**Table 1** Physicochemical parameters

S. no.	Parameter	Value			Reference	
		AHAC	AHAC + n(Zr-Ce-Sm) oxide	AHAC + n(Zr-Ce-Sm) oxide-Fe.Ali beads		
1	Moisture content (%)	6.84	5.41	5.12	Bureau of Indian Standards [16]	
2	Ash content (%)	4.53	3.85	3.54	Namasivayam and Kadirvelu [44]	
3	Iodine number (mg/g)	694	579	546	ASTM D4607–94 [10]	
4	Particle size (μ)	7.7	4.5	11.9	El-Hendawy et al. [22]	
5	Apparent density (g/mL)	0.293	0.312	0.326	Bureau of Indian Standards [16]	
6	BET surface area (m <sup>2</sup> /g)	Before:	264.3	367.8	398.5	Brunauer et al. [15]
		After:	201.5	196.9		

**Fig. 2** XRD patterns of **A** n(Zr-Ce-Sm) oxide, **B** AHAC, **C** AHAC + n(Zr-Ce-Sm) oxide and **D** AHAC + n(Zr-Ce-Sm) oxide-Fe.Ali beads



AHAC + n(Zr-Ce-Sm) oxide-Fe.Ali beads, were measured as per the standard procedures in the literature and the values are presented in the Table 1. The decrease in BET surface area indicates that the adsorption of lead and cadmium ions are 'on to' the surface of adsorbents.

### 3.1.2 XRD analysis

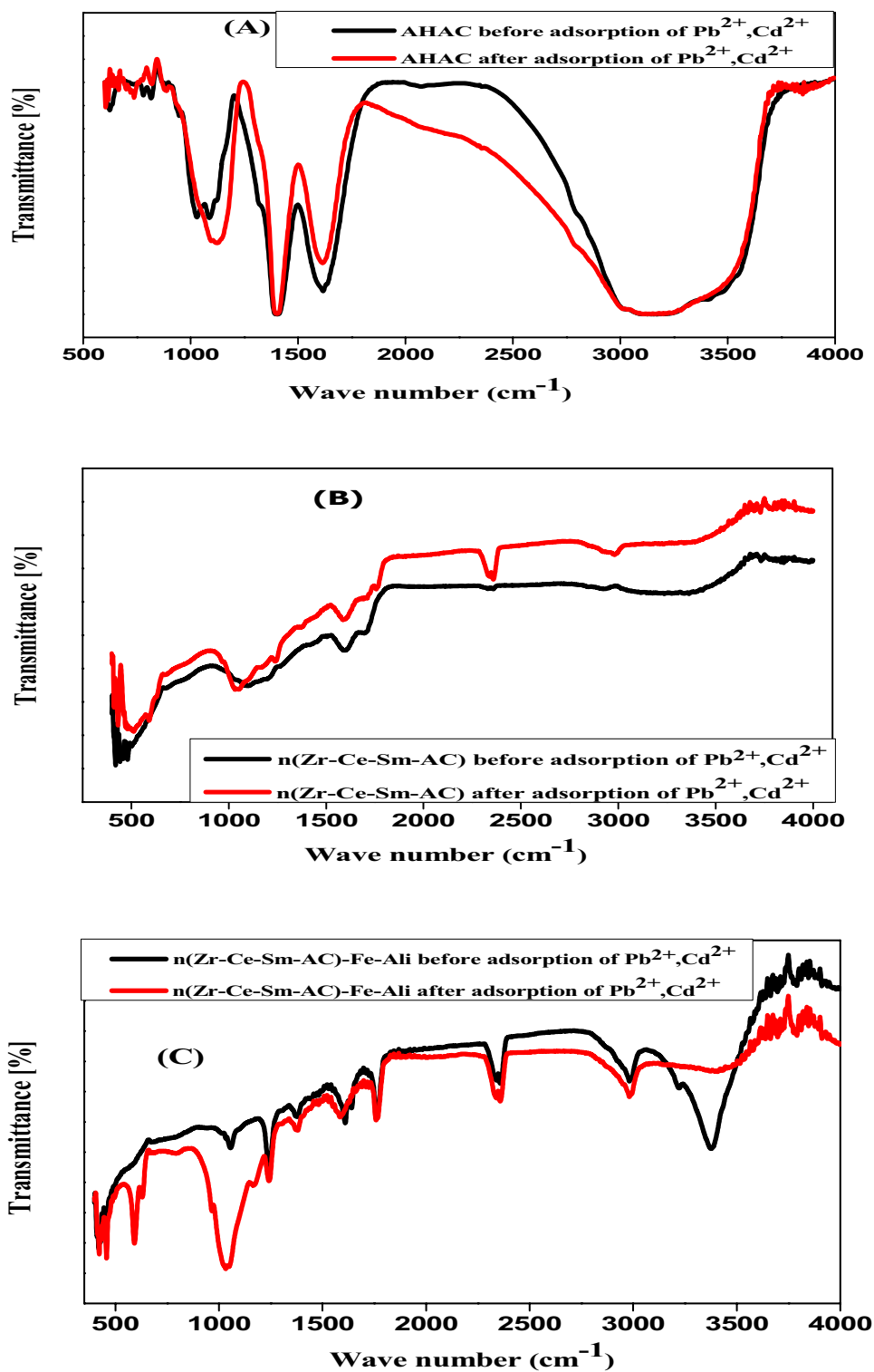
XRD patterns of n(Zr-Ce-Sm) oxide, AHAC, AHAC + n(Zr-Ce-Sm) oxide and AHAC + n(Zr-Ce-Sm) oxide-Fe.Ali beads are presented in Fig. 2. The mixed nanoparticles of (Zr-Ce-Sm) oxides (Fig. 2A) had shown empathic peaks at 2θ: 29.1°, 33.8°, 37.2°, 44.5°, 47.2°, 48.6°, 58.1°, 65.1° and 79.1°. It resembles JCPDS Card no 34–0394 [6]. Adopting Scherrer equation,  $L = \frac{k\lambda}{BCOS\theta}$ , the average crystallite size of the mixed metal oxide was evaluated as 11.7 nm [20] (Table S1).

The XRD spectrum of *Artocarpus heterophyllus* active carbon (AHAC) had shown a wide peak at 2θ = 22.6° and it is a characteristic of non-graphite carbon. Another 'sharp peak' at 2θ = 44.5° was noticed due to graphitic carbon (Fig. 2B). The broadness is indicative of the prevalence of more amorphous and structural irregularity regions.

It is interesting to note the changes occurred in the XRD spectral characteristics of AHAC when loaded with nano-mixed oxide on comparison with individual active carbon (AHAC) and nanoparticles (Fig. 2C). The AHAC + n(Zr-Ce-Sm) oxide had shown peaks at 2θ: 29.1°, 33.7°, 44.5°, 48.7°, 58.3° and 79.1° (Fig. 2C). It is interesting to note that the broad peak at 22.6° in the active carbon had turned to be sharp with the shift of peak position. The peaks at 37.2° and 65.1° present in the XRD spectrum of nano-mixed oxides are missing while the peaks at 47.2° have been shifted to 48.7°. These changes in the characteristics of peaks with respect to nature and position indicate that the nanometal oxide particles have interacted with the various functional groups present in the matrix of the active carbon.

The XRD spectrum of beads (AHAC + n(Zr-Ce-Sm) oxide-Fe.Ali) (Fig. 2D) had shown further marked variations in the spectral features at 2θ: 30.1°, 35.4°, 44.5°, 50.2°, 57.2° and 62.5°. Some of the peaks present in the 'AHAC + n(Zr-Ce-Sm) oxide' are missing and some are shifted with marked increase in the sharpness of the peaks. These features are emphatic proof that 'AHAC + n(Zr-Ce-Sm) oxide' is firmly embedded in the iron-alginate beads.

**Fig. 3** FTIR spectra of **A** AHAC, **B** AHAC + n(Zr-Ce-Sm) oxide and **C** AHAC + n(Zr-Ce-Sm) oxide-Fe.Ali beads before and after adsorption



### 3.1.3 FTIR analysis

FTIR spectra were taken ‘before and after’ adsorption of lead and cadmium ions for the adsorbents, AHAC, ‘AHAC + n(Zr-Ce-Sm)oxide’ and ‘AHAC + n(Zr-Ce-Sm)

oxide-Fe.Ali’ beads and presented in Fig. 3. As it can be seen from the figure, the spectra have several characteristic bands and each band represents specific functional groups present in the adsorbents.

Spectral features before adsorption are as follows:

**Fig. 4** FESEM images of AHAC: **A** before, **B** after; AHAC + n(Zr-Ce-Sm) oxide: **C** before, **D** after; AHAC + n(Zr-Ce-Sm) oxide-Fe.Ali beads: **E** before, **F** after adsorption of  $Pb^{2+}$  and  $Cd^{2+}$  ions

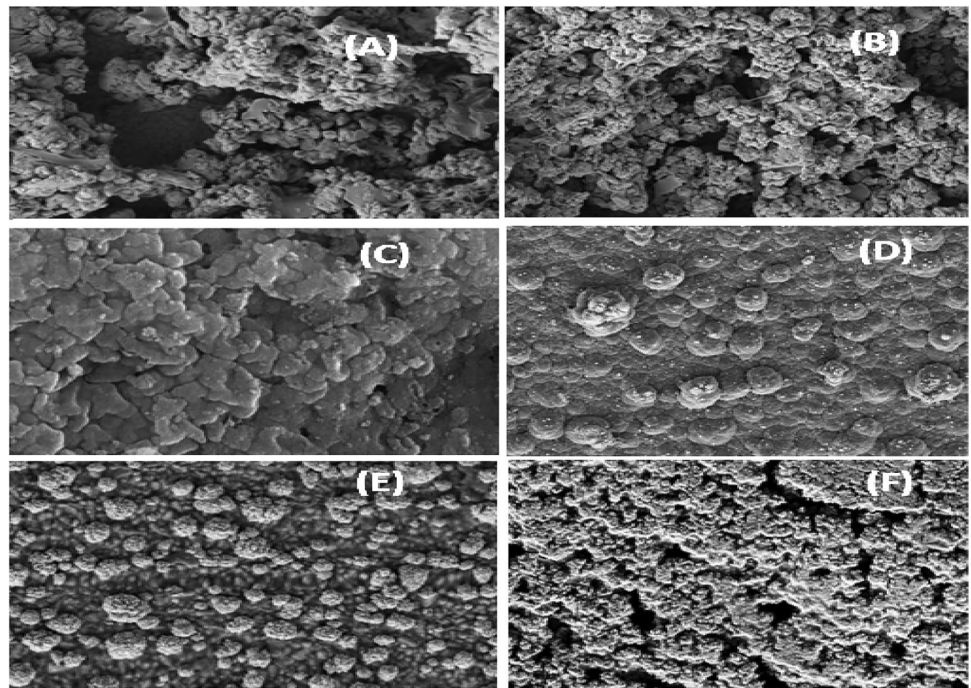


**Fig. 5** EDX images of AHAC: **A** before, **B** after; AHAC + n(Zr-Ce-Sm) oxide: **C** before, **D** after; AHAC + n(Zr-Ce-Sm) oxide-Fe.Ali beads: **E** before, **F** after adsorption of  $Pb^{2+}/Cd^{2+}$  ions

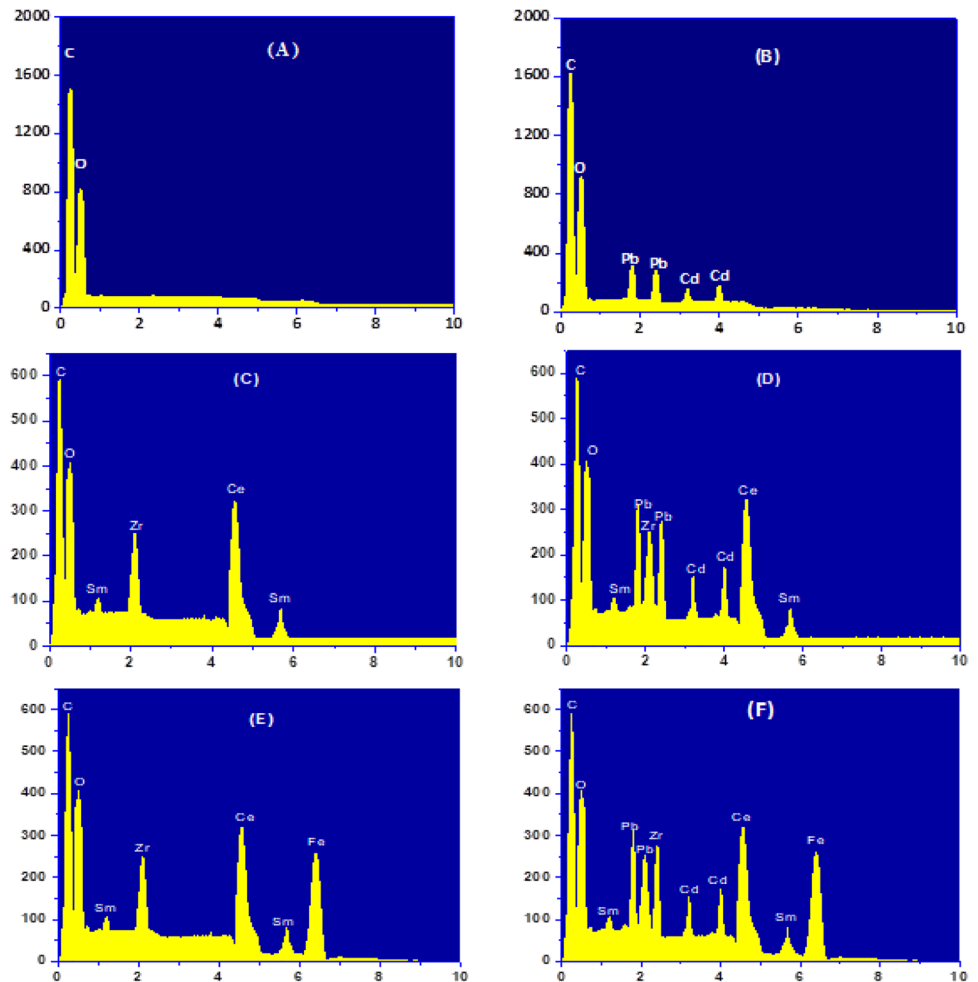
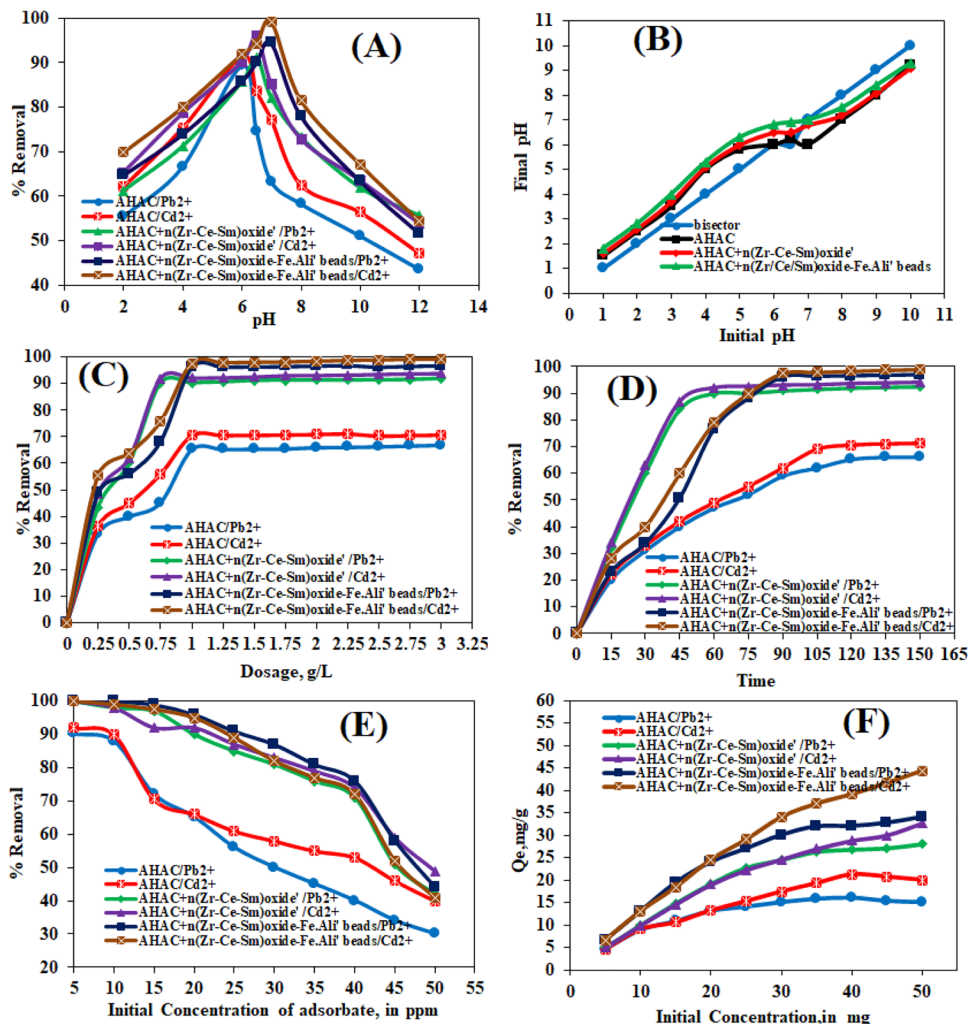


**Fig. 6** Effect of **A** pH, **B** pH<sub>zc</sub>, **C** dosage, **D** time of equilibration, **E** initial concentration of Pb<sup>2+</sup>/Cd<sup>2+</sup>, **F** sorption capacity of AHAC, AHAC + n(Zr-Ce-Sm)oxide and AHAC + n(Zr-Ce-Sm) oxide-Fe.Ali beads



- AHAC (Fig. 3A): (a) broad peak for symmetric stretching in the range 3000–3500 cm<sup>-1</sup> indicative of strong hydrogen bonding between the surface hydroxyl groups; (b) a strong peak at 1613 cm<sup>-1</sup> symmetric stretching of -O-C=O (ester); (c) a peak at 1403 cm<sup>-1</sup> — ‘C=C’ — symmetric stretching; (d) a peak at 1121 cm<sup>-1</sup> — ‘N-H’ symmetric tracings; (e) peaks at 1085 and 1029 cm<sup>-1</sup> — ‘C-O-’ stretching; (f) peaks at 947 cm<sup>-1</sup>, 883 cm<sup>-1</sup> and 615 cm<sup>-1</sup> — C-C- and -C-H- — deformations and/or di-substituted aromatic moiety of graphite carbon.
- AHAC + n(Zr-Ce-Sm) oxide (Fig. 3B): when the nano-mixed metal oxide is loaded on AHAC, there are marked changes in the spectral features: the broad peak pertains to -OH has been drastically reduced; new small peak at 2348 and 1761 cm<sup>-1</sup> of stretching frequencies of ‘-O-Sm=O/ O-Zr=O’ appeared [18], and the peaks at 1238 and 1043 cm<sup>-1</sup> pertaining to ‘C-O-’ stretching with reduced intensities. Furthermore, the

intensive peaks related to defamation vibrations of nanoparticles appeared below 850 cm<sup>-1</sup>: (a) 590 and 513 cm<sup>-1</sup> of ‘Zr-O/ Zr-OH’, (b) 525 and 528 cm<sup>-1</sup> of ‘-Sm-O/-Sm-OH’ and (c); 500 and 480 cm<sup>-1</sup> — of ‘Ce=O’ and/or ‘O-Ce=O’; and in addition small but emphatic peaks also observed at 469, 458, 441 432 and 418 cm<sup>-1</sup> pertaining to the meal oxides interactions with various functional groups.

- AHAC + n(Zr-Ce-Sm) oxide-Fe.Ali beads (Fig. 3C): when the active carbon loaded with mixed nano-metal oxide was embedded in iron-alginate beads, the prominent peaks observed are as follows: (a) a sharp and intensive peak at 3381 cm<sup>-1</sup> and a small but clear peak at 3220 cm<sup>-1</sup> (in contrast to the spectrum AHAC + n(Zr-Ce-Sm) oxide) — indicative of breaking of hydrogen bonding in the surface hydroxyl groups due to modification done by iron-alginate beading; (b) 2981 cm<sup>-1</sup> — symmetric stretch of CH<sub>2</sub>



**Fig. 7** Interference of co-ions: **A** co-cations and **B** co-anions

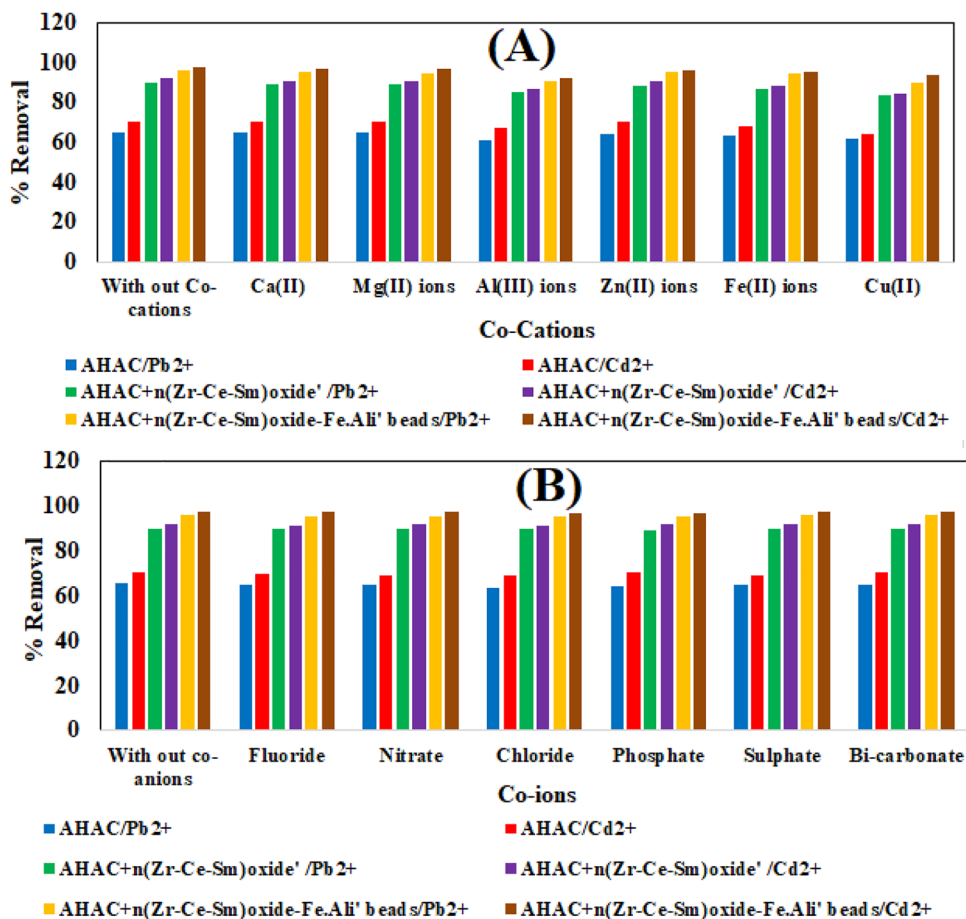
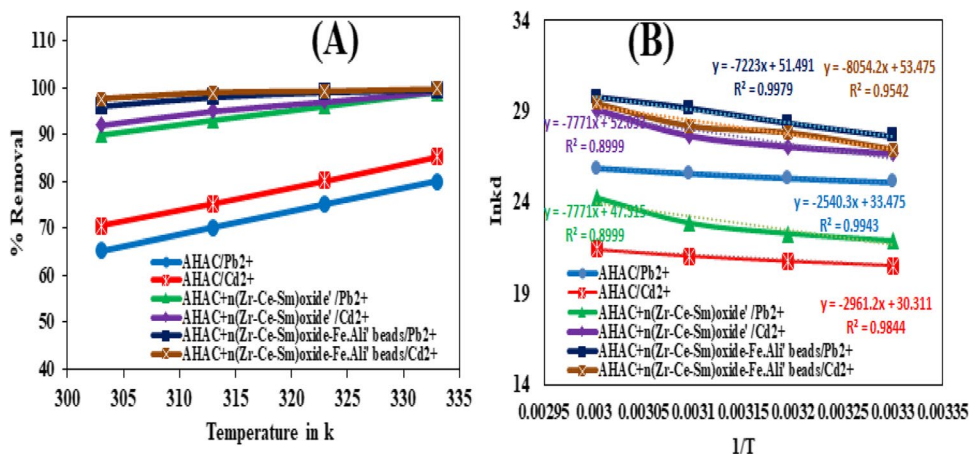


**Fig. 8** **A** Effect of Temperature on extraction of  $Pb^{2+}/Cd^{2+}$ ; **B** Vant Hoff's plots

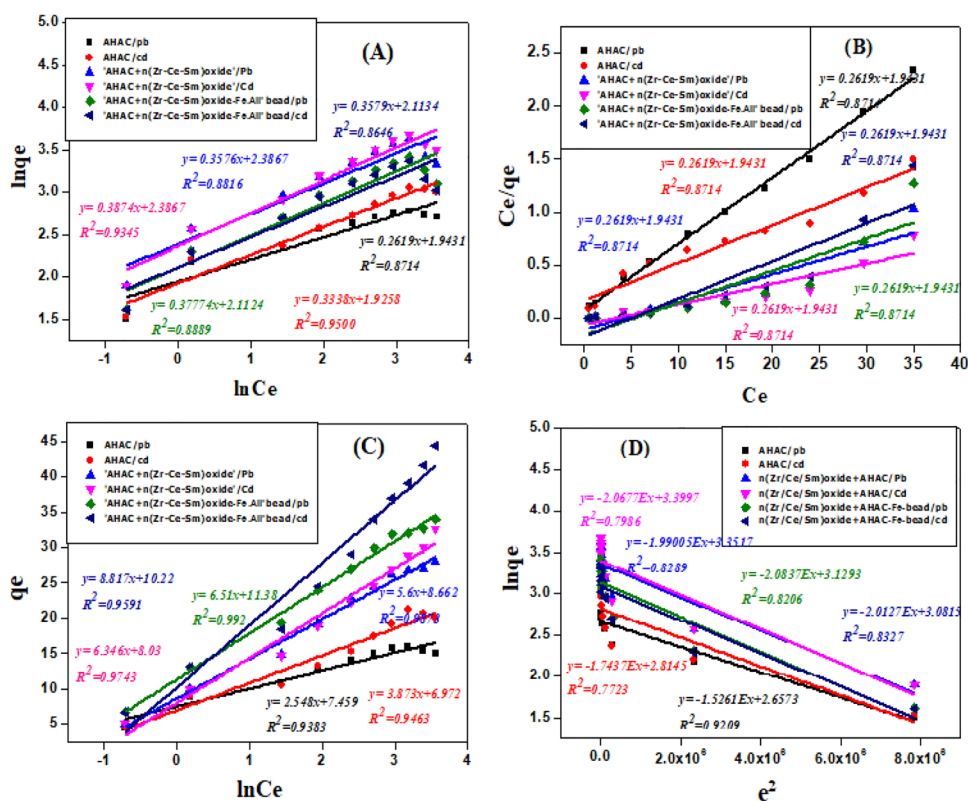


group in alginate moiety; (c) 1756, 1725, 1709 and 1692  $cm^{-1}$  — due to stretching vibrations of carbonyl and/or ester groups in the alginate moiety and also metal (Zr/Fe/Ce) carbonyls; (d) 1243 and 1052  $cm^{-1}$  — pertains to symmetric stretching vibrations of ‘-C-O-’ and/or ‘-Fe-O-’ (e) frequencies below 700  $cm^{-1}$ , namely, 457, 449, 439, 428, 419 and 411  $cm^{-1}$ , pertain to the defamation vibrations of ‘-Fe/Zr//Sm/Ce-O-’.

There are marked changes in the spectral features after adsorption of  $Pb^{2+}$  and  $Cd^{2+}$  ions above said three adsorbents as detailed hereunder:

- AHAC: (a) changes in the broadness of -OH peak; (b) three peaks pertaining to ‘-C-O’ and -N-H stretching yield to a single peak 1127  $cm^{-1}$  with increasing intensity; (c) additional sharp peaks of different intensities

**Fig. 9** Sorption isotherm models: **A** Freundlich model; **B** Langmuir model; **C** Temkin model; **D** Dubinin–Radushkevich model



at 883, 820, 777, 736 and  $720\text{ cm}^{-1}$  pertain to  $-\text{Cd}-\text{O}/\text{Cd}=\text{O}/-\text{Cd}-\text{OH}$  deformation stretching and (e) furthermore, additional sharp bands of varying intensities at 677, 664, 653 and  $646\text{ cm}^{-1}$  pertaining  $-\text{Pb}-\text{O}/-\text{Pb}-\text{O}-\text{H}/\text{Pb}=\text{O}$  deformation stretching.

- AHAC + n(Zr-Ce-Sm) oxide: (a) a sharp band appeared at  $3160\text{ cm}^{-1}$  with decrease in broadness of the stretching frequencies related to hydroxyl groups, indicating the collapse of inter hydrogen bonding (b) emphatic peaks appeared at 2348 and 1761 pertaining to stretching vibrations of  $\text{O}=\text{Pb}(\text{Cd})-\text{O}/\text{O}=\text{Pb}(\text{Cd})-\text{O}-\text{H}\text{ cm}^{-1}$  (c) additional peaks 590 and  $513\text{ cm}^{-1}$  pertaining to the deformation vibrations of  $-\text{O}-\text{Pb}/\text{Cd}=\text{O}$ .
- AHAC + n(Zr-Ce-Sm) oxide-Fe.Ali beads: (a) a strong  $-\text{OH}$  peak at  $3456\text{ cm}^{-1}$  with marked variations in the features; (b) strong peaks at 2352 and 1761, indicative of metal carbonyl groups; strong peaks at 1174 and  $1035\text{ cm}^{-1}$ , indicating the interaction of  $-\text{C}-\text{O}-$  groups with  $\text{Pb}^{2+}$  and  $\text{Cd}^{2+}$ ; additional strong peaks at 621 and  $592\text{ cm}^{-1}$  pertaining to  $-\text{O}-\text{Pb}/\text{Cd}=\text{O}$  deformation vibrations along with the 495, 485, 456, 438, 430 and  $421\text{ cm}^{-1}$  peaks pertaining to the deformation peaks of  $(\text{Zr}/\text{Ce}/\text{Sm})-\text{C}=\text{O}$  or  $\text{H}-\text{O}(\text{Zr}/\text{Ce}/\text{Sm})-\text{C}-\text{O}-\text{H}$ .

These variations in spectral characteristics observed ‘before and after’ adsorption of  $\text{Pb}^{2+}$  and  $\text{Cd}^{2+}$  amply

indicate the interaction of  $\text{Pb}^{2+}$  and  $\text{Cd}^{2+}$  with the functional groups of the adsorbents and forming a kind of surface complex.

### 3.1.4 FESEM analysis

FESEM images of the adsorbents, AHAC, ‘AHAC + n(Zr-Ce-Sm)oxide’ and ‘AHAC + n(Zr-Ce-Sm) oxide-Fe.Ali’ beads, were taken before and after adsorption of  $\text{Pb}^{2+}/\text{Cd}^{2+}$  ions and presented in Fig. 4. Emphatic changes are observed when contrasting the features of images taken ‘before and after’ adsorption of  $\text{Pb}^{2+}$  and  $\text{Cd}^{2+}$ . AHAC image is endowed with voids, many boundaries and large edges but these features are reduced to some extent to turn the surface smooth after  $\text{Pb}^{2+}/\text{Cd}^{2+}$  sorption (Fig. 4A and B). Note-worthy changes can be observed in the surface features of images of ‘AHAC + n(Zr-Ce-Sm) oxide’ taken before and after  $\text{Pb}^{2+}/\text{Cd}^{2+}$  adsorption (Fig. 4C and D). Voids, edges, clear embedded nanoparticles and rough surface observed in before image are drastically reduced to increase in smoothness of the surface in the after adsorption image.

The image of ‘AHAC + n(Zr-Ce-Sm) oxide-Fe.Ali beads’ taken before sorption is endowed with circular shaped entities with many boundaries, some voids and many corners (Fig. 4E). These features are vanished

**Fig. 10** Adsorption kinetics: **A** pseudo-1st order kinetics; **B** pseudo-2nd order kinetics; **C** Elovich model; **D** Bangam’s pore diffusion models

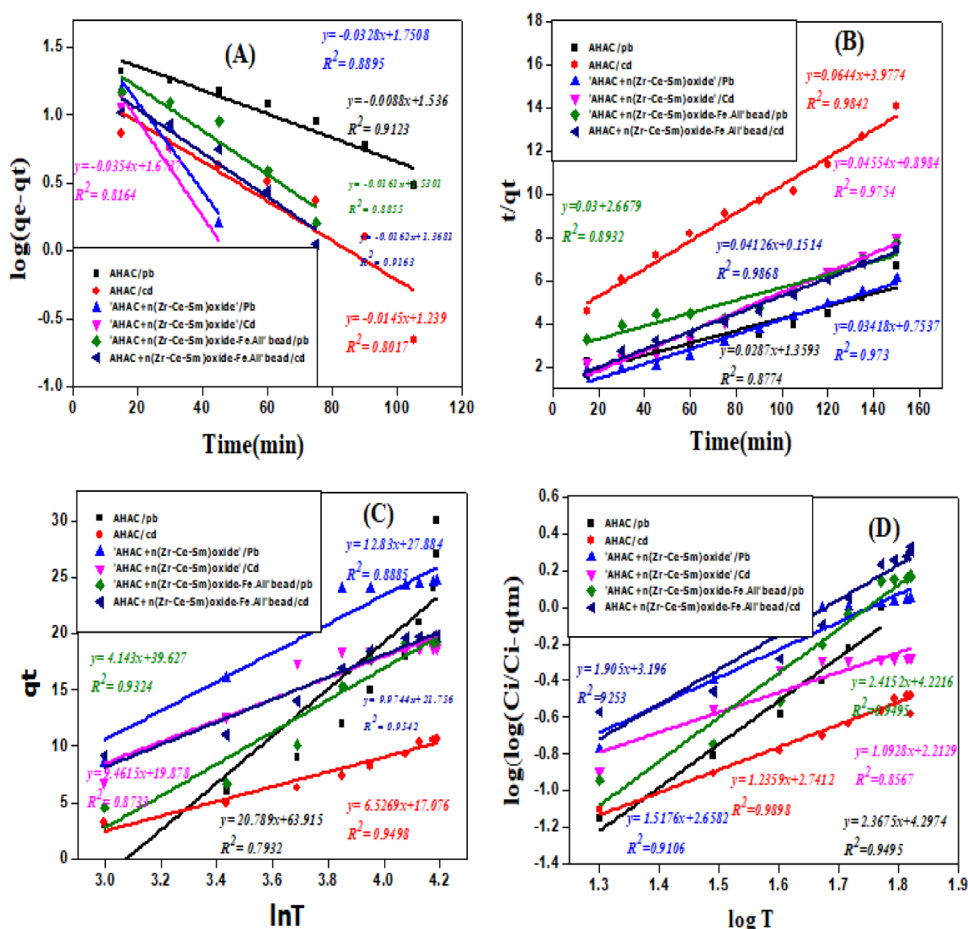
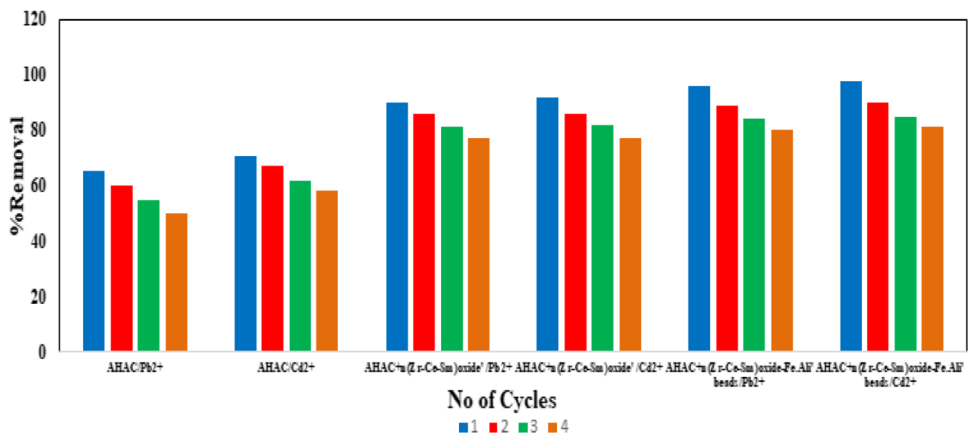


**Fig. 11** Regeneration studies



or partly reduced yielding a highly contrasting surface features after the sorption of Pb<sup>2+</sup>/Cd<sup>2+</sup> (Fig. 4F). These surface morphological changes in the surface characteristics are indicative of adsorption of Pb<sup>2+</sup> and/or Cd<sup>2+</sup> ions by AHAC, ‘AHAC + n(Zr-Ce-Sm) oxide’ and ‘AHAC + n(Zr-Ce-Sm) oxide-Fe.Ali beads’.

### 3.1.5 EDX spectral analysis

The spectra observed for the three adsorbents (AHAC, ‘AHAC + n(Zr-Ce-Sm) oxide’ and ‘AHAC + n(Zr-Ce-Sm) oxide-Fe.Ali’ beads) before and after adsorption of Pb<sup>2+</sup> and Cd<sup>2+</sup> are presented in Fig. 5.

**Table 2** Simultaneous removal lead and cadmium ions\*

Samples	Concentration of mixture lead + cadmium (mg/L)		After adsorption mg/L		% Removal	
A: AHAC: optimum conditions: pH: 6.0; dosage of activated carbon: 1.5 g/L; contact time: 120 min; rpm: 350; Temp.: 30 ± 1 °C)						
	Pb <sup>2+</sup>	Cd <sup>2+</sup>	Pb <sup>2+</sup>	Cd <sup>2+</sup>	Pb <sup>2+</sup>	Cd <sup>2+</sup>
1	5.2	2.4	0.0	0.0	100	100
2	5.8	2.7	0.0	0.0	100	100
3	6.9	3.3	0.0	0.0	100	100
4	7.4	3.9	0.0	0.0	100	100
5	8.1	4.5	0.0	0.0	100	100
B: AHAC + n(Zr-Ce-Sm) oxide: optimum conditions: pH: 6.5; dosage of composite: 1.25 g/L; contact time: 60 min; rpm: 350; Temp.: 30 ± 1 °C)						
1	5.2	2.4	0.0	0.0	100	100
2	5.8	2.7	0.0	0.0	100	100
3	6.9	3.3	0.0	0.0	100	100
4	7.4	3.9	0.0	0.0	100	100
5	8.1	4.5	0.0	0.0	100	100
C: AHAC + n(Zr-Ce-Sm) oxide-Fe.Ali beads: optimum conditions: pH:7.0; dosage of composite: 1.5 g/L; contact time: 90 min; rpm: 350; Temp.: 30 ± 1 °C)						
1	5.2	2.4	0.0	0.0	100	100
2	5.8	2.7	0.0	0.0	100	100
3	6.9	3.3	0.0	0.0	100	100
4	7.4	3.9	0.0	0.0	100	100
5	8.1	4.5	0.0	0.0	100	100

\*The values are average of five estimations; *SD* ± 0.18

**Table 3** Thermodynamic parameters

Adsorbent	$\Delta H^0$ (kJ/mol)	$\Delta S^0$ (J/mol)	$\Delta G^0$ (kJ/mol)				$R^2$
			303 K	313 K	323 K	333 K	
AHAC	18.64	232.23	-51.72	-54.05	-56.37	-58.69	0.993
AHAC + n(Zr-Ce-Sm) oxide	34.58	292.16	-53.92	-56.86	-59.78	-62.7	0.994
AHAC + n(Zr-Ce-Sm) oxide-Fe.Ali beads	53.79	357.12	-54.41	-57.98	-61.55	-65.12	0.983

As it can be seen from the Fig. 5, peaks pertaining to Pb<sup>2+</sup> and Cd<sup>2+</sup> were present in the EDX spectra of the adsorbents after adsorption of Pb<sup>2+</sup> and Cd<sup>2+</sup> ions. Whereas, these peaks were absent in the EDX spectra of the adsorbents before adsorption. Hence, the results of EDX spectra confirmed the adsorption of Pb<sup>2+</sup> and Cd<sup>2+</sup> ions onto AHAC, 'AHAC + n(Zr-Ce-Sm) oxide' and 'AHAC + n(Zr-Ce-Sm) oxide-Fe.Ali' beads.

### 3.2 Extraction parameters

Different experimental conditions such as pH, adsorbent dosage, agitation time, initial metal ion concentrations and temperature were varied to investigate the maximum extraction of lead and cadmium ions by the adsorbents, AHAC, 'AHAC + n(Zr-Ce-Sm) oxide' and AHAC + n(Zr-Ce-Sm) oxide-Fe.Ali beads.

#### 3.2.1 Effect of initial pH

The adsorption process was influenced by the pH of the solution. The effect of initial pH of the solution is as shown in Fig. 6A. The pH<sub>ZPC</sub> values of the adsorbents were established as per the standard methods in the literature [14] and are presented in Fig. 6B. The pH<sub>ZPC</sub> values were 6.0, 6.5 and 7.0 for AHAC, 'AHAC + n(Zr-Ce-Sm) oxide' and 'AHAC + n(Zr-Ce-Sm) oxide-Fe.Ali beads', towards lead and cadmium respectively.

When the solution pH was equal to pH<sub>ZPC</sub>, the surface of the adsorbents was neutral. Below these pH<sub>ZPC</sub> values, the surface was surrounded by mostly H<sup>+</sup> ions and so imparting positive charge to the surface. Above these values, deprotonation of surface functional groups occurs, imparting negative charge to the surface [14].

**Table 4** Evaluated adsorption isothermal parameters

Adsorbate	Parameter	Freundlich isotherm	Langmuir isotherm	Temkin isotherm	Dubinin-Radushkevich isotherm
AHAC/Pb <sup>2+</sup>	Slope	0.262	0.062	2.548	- 1.52
	Intercept	1.9431	0.078	7.439	2.65
	R <sup>2</sup>	0.8714	0.986	0.9382	0.9209
		1/n=0.262	R <sub>L</sub> =0.05	B=2.548	E=1.06 kJ/mol
AHAC/Cd <sup>2+</sup>	Slope	0.334	0.036	3.873	- 1.74
	Intercept	1.9258	0.163	6.972	2.81
	R <sup>2</sup>	0.9500	0.9750	0.9463	0.7723
		1/n=0.334	R <sub>L</sub> =0.23	B=3.873	E=1.2 kJ/mol
AHAC + n(Zr-Ce-Sm)oxide/Pb <sup>2+</sup>	Slope	0.3576	0.026	6.497	- 1.99
	Intercept	2.386	0.1105	11.914	3.35
	R <sup>2</sup>	0.958	0.8317	0.8475	0.8289
		1/n=0.357	R <sub>L</sub> =0.17	B=6.497	E=1.4 kJ/mol
AHAC + n(Zr-Ce-Sm)oxide/Cd <sup>2+</sup>	Slope	0.387	0.019	7.4390	- 2.06
	Intercept	2.3867	0.065	11.281	3.39
	R <sup>2</sup>	0.975	0.8522	0.9189	0.7986
		1/n=0.387	R <sub>L</sub> =0.63	B=7.439	E=1.48 kJ/mol
AHAC + n(Zr-Ce-Sm) oxide-Fe.Ali beads/Pb <sup>2+</sup>	Slope	0.377	0.030	5.417	- 2.08
	Intercept	2.1124	0.163	9.081	3.12
	R <sup>2</sup>	0.969	0.7764	0.8540	0.8206
		1/n=0.377	R <sub>L</sub> =0.83	B=5.417	E=1.47 kJ/mol
AHAC + n(Zr-Ce-Sm) oxide-Fe.Ali beads/Cd <sup>2+</sup>	Slope	0.358	0.036	4.909	- 2.01
	Intercept	2.1134	0.176	9.177	3.08
	R <sup>2</sup>	0.956	0.8091	0.8271	0.8327
		1/n=0.358	R <sub>L</sub> =0.25	B=4.909	E=1.42 kJ/mol

**Table 5** Evaluated adsorption kinetical models

Adsorbents	Parameters	Pseudo-first order model	Pseudo-second order model	Elovich model	Bangham's pore diffusion model
AHAC/Pb <sup>2+</sup>	Slope	0.009	0.028	20.789	2.367
	Intercept	1.536	1.359	63.915	4.297
	R <sup>2</sup>	0.8774	0.9123	0.7932	0.9495
AHAC/Cd <sup>2+</sup>	Slope	0.015	0.064	6.527	1.235
	Intercept	1.239	3.977	17.076	2.741
	R <sup>2</sup>	0.8017	0.9842	0.9498	0.9498
AHAC + n(Zr-Ce-Sm) oxide/Pb <sup>2+</sup>	Slope	0.033	0.0342	12.83	1.517
	Intercept	1.751	0.754	27.88	2.658
	R <sup>2</sup>	0.8895	0.9730	0.8885	0.9106
AHAC + n(Zr-Ce-Sm) oxide/Cd <sup>2+</sup>	Slope	0.035	0.045	9.461	1.093
	Intercept	1.673	0.898	19.878	2.212
	R <sup>2</sup>	0.8164	0.9754	0.8733	0.8567
AHAC + n(Zr-Ce-Sm) oxide-Fe.Ali beads/Pb <sup>2+</sup>	Slope	0.016	0.03	14.143	2.415
	Intercept	1.530	2.667	39.627	4.221
	R <sup>2</sup>	0.8855	0.9878	0.9324	0.9495
AHAC + n(Zr-Ce-Sm) oxide-Fe.Ali beads/Cd <sup>2+</sup>	Slope	0.0162	0.041	9.974	1.905
	Intercept	1.368	1.151	21.75	3.196
	R <sup>2</sup>	0.9163	0.9868	0.9542	0.9698

**Table 6** Applications

Samples	Initial conc. of ions, $C_i$ (mg/L)		Conc. of ions after treatment, $C_e$ (mg/L)		% Removal	
	Lead	Cadmium	Lead	Cadmium	Lead	Cadmium
A: AHAC as adsorbent: optimum conditions: pH: 6.0; dosage of active carbon: 1.0 g/L; contact time: 120 min; rpm: 350; Temp.: $30 \pm 1$ °C)						
1	1.8	5.7	0	0	100	100
2	3.15	9.2	0	0	100	100
3	4.4	11.3	0	0	100	100
4	5.9	17.2	0	0.087	100	99.7
5	6.5	19.4	0.014	0.355	99.8	98.7
B: AHAC + n(Zr-Ce-Sm) oxide as adsorbent: Optimum conditions: pH: 6.5; dosage of composite: 0.75 g/L; contact time: 60 min; rpm: 350; Temp.: $30 \pm 1$ °C)						
1	1.8	5.7	0	0	100	100
2	3.15	9.2	0	0	100	100
3	4.4	11.3	0	0	100	100
4	5.9	17.2	0	0.096	100	99.8
5	6.5	19.4	0.017	0.358	99.9	98.8
C: AHAC + n(Zr-Ce-Sm) oxide-Fe.Ali beads as adsorbent: Optimum conditions: pH: 7.0; dosage of composite: 1.0 g/L; contact time: 90 min; rpm: 350; Temp.: $30 \pm 1$ °C)						
1	1.8	5.7	0	0	100	100
2	3.15	9.2	0	0	100	100
3	4.4	11.3	0	0	100	100
4	5.9	17.2	0	0	100	100
5	6.5	19.4	0	0	100	100

\*Mean of six estimations;  $SD \pm 0.19$ **Table 7** Comparison of adsorbents

S. no.	Sorbent	pH	Contact time (min)	Pollutant	Adsorption capacity (mg/g)	Reference
1	Polyphenolic bioactive Indian curry leaf ( <i>Murraya koengii</i> ) powder	4.5	50	Lead	13.62	Mukherjee et al. [41]
2	HNO <sub>3</sub> -treated lignite-activated carbon (NAC)	7.2		Cadmium	22.8	Sun et al. [55]
3	Activated polyacrylonitrile	5.0	60	Lead	12.7	Amin et al. [7]
4	Activated carbon prepared from African palm fruit	8.0	60	Cadmium	1.82	Abdulrazak et al. [1]
5	Lignite, Drama, northern Greece	4.5	720	Cadmium	25.5	Pentari and Vamvouka [46]
6	Stem powders of <i>Calophyllum inophyllum</i> (CISP)	6.5	75	Lead	14.9	Sneha Latha et al. [51]
		7.0	75	Cadmium	16.2	
7	Activated carbon of <i>Calophyllum inophyllum</i> (CISAC)	6.5	120	Lead	17.0	
		7.0	120	Cadmium	18.5	
8	<i>L. leucocephala</i> -extracted polyphenols (LLEPs)	5.1	120	Lead	21.552	Mukul et al. [42]
			120	Cadmium	16.807	
9	Activated carbon from black cumin seeds	9.0	60	Lead	17.98	Thabede et al. [63]
10	Gelatin sponge	6.0		Cadmium	9.35	Li et al. [37]
				Lead	9.75	
11	Microwaved olive stone-activated carbon activated	5.0	180	Cadmium	11.7	Alslaibi et al. [5]
12	AHAC	6.0	120	Lead	15.0	Present work
		6.0	120	Cadmium	20.0	
13	AHAC + n(Zr-Ce-Sm) oxide	6.5	60	Lead	28.0	
		6.5	60	Cadmium	32.6	
14	AHAC + n(Zr-Ce-Sm) oxide-Fe.Ali beads	7.0	90	Lead	34.0	
		7.0	90	Cadmium	44.3	

The optimum pH values for the maximum extraction of lead and cadmium ions were 6.0; 6.5 and 7.0 with the adsorbents, AHAC; ‘AHAC + n(Zr-Ce-Sm) oxide’ and ‘AHAC + n(Zr-Ce-Sm) oxide-Fe.Ali beads’ respectively. As these values were equal to the pHzpc values, the surfaces of the adsorbents were neutral. At these pH values, lead exists as  $Pb^{2+}/PbOH^+$  while major species of cadmium as  $Cd^{2+}$  (with traces of  $CdOH^+$ ). Hence, the mechanism of the adsorption process was not due to the simple electrostatic interactions between the metal ions and the adsorbent surface. But may be due to the formation of surface complex and/or ion-exchange mechanism between  $Pb^{2+}/Cd^{2+}$  with the surface functional groups of adsorbents [51]. The high values of  $\Delta H^0$  supported the interaction between adsorbent surface and metal ions were under ion exchange process [8].

At low pH values, the decrease in % removal was due to repulsive interaction between the protonated positively charged adsorbents surface and  $Pb^{2+}/Cd^{2+}$  cations [23]. The decrease in % removal at higher pH values was due to the negative charge of adsorbents surface by deprotonation and the presence of negatively charged lead and cadmium ions in the solution:  $Pb(OH)_3^-$ ,  $Pb(OH)_4^{2-}$ ,  $(Cd(OH)_3)^-$ ,  $(Cd(OH)_4)^{2-}$  [8, 49].

### 3.2.2 Effect of sorbents dosage

The effect of adsorbent dosage on the extraction of lead and cadmium ions is presented in Fig. 6C. It was interesting to note that the % removal of lead and cadmium ions was increased almost linearly as the dosage of the adsorbents was increased up to a certain dosage and after that, there was no marked extraction, i.e. a steady state was reached. Thus, the optimum dosages for the maximum extraction of lead and cadmium ions were found to be 1.0 g/L in the case of AHAC and beads and 0.75 g/L with ‘AHAC + n(Zr-Ce-Sm)oxide’. At these optimum concentrations, the maximum  $Pb^{2+}/Cd^{2+}$  extractions were as follows: 65.2/70.5% with AHAC, 90.0/92.0% with ‘AHAC + n(Zr-Ce-Sm) oxide’ and 96.0/97.5% with beads.

The progressive increase of extraction with increase in the dosage of the adsorbents was due to the availability of more active sites at higher doses of the adsorbents [33]. This seems to be correct up to certain optimum dosages. But after that, there was a non-significant increase in percent removal. This suggested the possibility of particle aggregation, closings and/or restricting of pathways for the adsorbate ions to reach to the active sites, which lead to the decrease in surface area of the adsorbents and hence, steady states were resulted [33].

### 3.2.3 Effect of contact time

The removal of lead and cadmium ions from water by the batch adsorption process was evidently a time-dependent process and the results are presented in Fig. 6D. The maximum Pb/Cd extractions were attained at 120 min for AHAC, 60 min for nanocomposite with AHAC and 90 min for beads. Hence, these times were considered to be as optimum equilibration times. As is evident from the figures, the rate of metal ions removal was very rapid at the beginning of the adsorption process because of the availability of more surface area for the adsorption of metal ions [52, 59]. But with progress of time, the active sites were increasingly used-up and hence, the rate of sorption was mellowed. As the dosage of adsorbents was fixed, steady states were observed when all the active sites were spent out [52, 59].

### 3.2.4 Effect of initial $Pb^{2+}/Cd^{2+}$ concentrations

The effect of initial concentration of lead and cadmium on % removal was investigated with the adsorbents, AHAC, ‘AHAC + n(Zr-Ce-Sm)oxide’ and ‘AHAC + n(Zr-Ce-Sm) oxide-Fe.Ali’ beads and the results are presented in Fig. 6E and F.

From these plots, it was observed that the percent removal decreases with increase in initial concentrations of metal ions, while the amounts of metal ions uptake (adsorption capacities,  $q_e$ ) by the adsorbents were increased [53, 60].

As the doses of the adsorbents were fixed, the available binding sites on the surface of the adsorbents were also fixed. Due to this, at lower concentrations, metal ions had needed number of active sites for interactions and facilitated high adsorption, while at higher concentrations, more metal ions were left unadsorbed because of the unavailability of the binding sites and thus decreased in percent removal [53, 60].

The increase in adsorption capacities as the metal ion concentration raises, may be accounted from the fact that the metal ion concentration on the surface of the adsorbents differ from the bulk of the solution. This concentration gradient will be more with increase in metal ion concentrations, and this causes a kind of driving force for metal ions moving faster towards the surface of adsorbents and hence higher adsorptivities at higher metal ion concentrations [31, 49, 56].

### 3.2.5 Interference of co-ions

Interference of co-ions was investigated on the extraction of lead and cadmium ions with fourfold excess of common ions and the results are presented in Fig. 7A and B.

As it can be seen from the figure, in presence of common cations and anions, the extractions of lead and

cadmium ions were effected marginally [51]. Some factors such as size, charge, electro negativity, polarizability, and forces between the ions may describe the extent of interference on the extraction of  $Pb^{2+}$  and  $Cd^{2+}$  ions [45].

### 3.3 Simultaneous removal of lead and cadmium ions

The optimum conditions for the maximum extraction of lead and cadmium ions were established with initial concentration of metal ion solutions:  $Pb^{2+}$  (20.0 mg/L) and  $Cd^{2+}$  (15.0 mg/L) at pH: 6.0, 6.5 and 7.0; sorbent dosage: 1.0, 0.75 and 1.0 g/L; agitation time: 120, 60 and 90 min for AHAC, 'AHAC + n(Zr-Ce-Sm) oxide' and 'AHAC + n(Zr-Ce-Sm) oxide-Fe.Ali' beads respectively at a temperature of 30 °C. To assess whether these optimum conditions were also good enough to the simultaneous removal of lead and cadmium ions at the said pH values, experiments were conducted with simulated solutions of the admixtures of lead and cadmium ions.

The observations revealed that adsorbent dosage was to be increased while all other parameters were remained constant. Therefore, both the metal ions were effectively extracted simultaneously at the established extraction conditions, except dosage. The required adsorbent dosage in simultaneous removal of lead and cadmium ions was found to be 1.5, 1.25 and 1.5 g/L for AHAC, 'AHAC + n(Zr-Ce-Sm) oxide' and 'AHAC + n(Zr-Ce-Sm) oxide-Fe.Ali' beads respectively. The results are noted in Table 2.

### 3.4 Thermodynamic parameters

The effect of solution temperature on extraction process was studied and the results are presented in Fig. 8A.

As shown in the figure, the extraction of lead and cadmium ions was increased with increase in temperature. This was due to the increase in diffusion of metal ions towards the adsorbent surface and thus, more ions were penetrated into the matrix of adsorbent and hence high adsorption [47].

The values of thermodynamic parameters such as,  $\Delta G^0$ ,  $\Delta H^0$  and  $\Delta S^0$  were determined from the following equations [38, 47]:

$$\Delta G^0 = -RT \ln K_d$$

$$\ln K_d = \Delta S^0 / R - \Delta H^0 / RT$$

$$K_d = q_e / C_e$$

$$\Delta G^0 = \Delta H^0 - T \Delta S^0$$

where  $K_d$  is the distribution coefficient;  $q_e$  is the sorbed amount of  $Pb^{2+}/Cd^{2+}$ ;  $C_e$  is the equilibrium  $Pb^{2+}/Cd^{2+}$  concentration;  $T$  is the temp (K);  $R$  is the gas constant. The results are presented in Fig. 8B and Table 3.

From the table, it was observed that the  $\Delta G^0$  values were negative while  $\Delta H^0$  and  $\Delta S^0$  values were positive. The negative  $\Delta G^0$  values confirmed the spontaneous nature of adsorption of metal ions onto the adsorbents [12]. The enhanced adsorption attained at higher temperature was confirmed by the higher negative values of  $\Delta G^0$  at high temperatures [43].

The positive values of  $\Delta H^0$  confirmed the overall adsorption of lead and cadmium ions was endothermic and the high values of  $\Delta H^0$  supported the formation of surface complex and/or ion-exchange mechanism between  $Pb^{2+}/Cd^{2+}$  ions with the surface functional groups of adsorbents due to strong interactions between them [8, 51].

The positive and high values of  $\Delta S^0$  indicated the increased randomness at adsorbent-adsorbate interfaces during the adsorption process and also confirmed the favourability of the adsorbents towards lead and cadmium ions and thus resulted in high adsorption [8]. The similar observations were reported in the removal of toxic ions from polluted water [13, 51, 58].

### 3.5 Adsorption isotherms

To describe the adsorption behaviour of metal ions on the surface of the adsorbents, AHAC, 'AHAC + n(Zr-Ce-Sm) oxide' and 'AHAC + n(Zr-Ce-Sm) oxide-Fe.Ali' beads, isothermal study was carried out. The equilibrium adsorption data was analysed with Freundlich [25], Langmuir [35], Temkin and Pyzhev [62] and Dubinin-Radushkevich [21] models. The values of various parameters of the models were calculated. The results are presented in Fig. 9 and Table 4.

The correlation coefficient ( $R^2$ ) values close to unity confirmed the best fit model to the adsorption data [11, 39]. In the case of AHAC, as  $R^2$  values of Langmuir plot were close to unity than other models and so, the adsorption data was fitted well to the Langmuir isotherm model. This supported the uniform and monolayer adsorption of lead and cadmium ions onto the adsorbent surface. The similar results were observed in the removal of toxic ions from waste water [13, 51, 58]. Furthermore, the separation factor ( $R_L$ ) values were in between 'zero' to 1.0 and as per Hall et al. [27], the Langmuir isotherm sorption was favoured.

In the case of adsorbents, 'AHAC + n(Zr-Ce-Sm) oxide' and 'AHAC + n(Zr-Ce-Sm) oxide-Fe.Ali' beads, the  $R^2$  values of Freundlich plots were close to unity than other models. This indicated that the adsorption data was fitted well to the Freundlich isotherm model. This model supported the



non-uniform and multilayer adsorption of lead and cadmium ions onto the heterogeneous surface of the adsorbents [2]. Temkin and Dubinin–Radushkevich equations were used to calculate B and E values respectively and the results are presented in Table 4.

### 3.6 Adsorption kinetics

In this study, different kinetic models such as pseudo-1st and 2nd order and Elovich and Bangham's pore diffusion [4, 17, 28, 34] were used to analyse the experimental data to find the best fit model of adsorption of lead and cadmium ions using AHAC, 'AHAC + n(Zr-Ce-Sm) oxide' and 'AHAC + n(Zr-Ce-Sm) oxide-Fe.Ali' beads as adsorbents. The experimentally investigated results are presented in Fig. 10 and Table 5.

The correlation coefficient ( $R^2$ ) values reveal the best fitting kinetic model [11]. As it can be seen from the table, the correlation co-efficient ( $R^2$ ) values of pseudo-second order kinetics were close to unity for the adsorption of lead and cadmium ions by the adsorbents, 'AHAC + n(Zr-Ce-Sm) oxide' (Pb: 0.9730, Cd: 0.9754) and 'AHAC + n(Zr-Ce-Sm) oxide-Fe.Ali' beads (Pb: 0.9878, Cd: 0.9868). The adsorption of cadmium ions with the adsorbent AHAC (Cd: 0.9842) also fitted with pseudo-second order kinetics. But in the case of adsorption of lead ions by AHAC, the adsorption process was fitted with Bangham's pore diffusion model (Pb: 0.9495). Thus, the pseudo-second order model was the best fitted model compared to the other kinetic models in all adsorption process except the adsorption of lead ions by AHAC. The adsorption process that follows pseudo-second order kinetics indicating that the rate determining step may be the chemisorption process and it requires the interchange or involvement of electrons. The similar results were noticed in the previous works reported in the literature [3, 29, 30].

### 3.7 Regeneration of spent adsorbents

Solutions of different concentrations of acids, bases, salts and their blends were examined for the regeneration of used adsorbents. A 0.1 N HCl was found to be an effective desorbing agent in the regeneration of lead/cadmium ion-loaded adsorbents. The hydrochloric acid is used as a most efficient desorbing agent in the regeneration of various heavy metal ion-loaded adsorbents [36, 40, 61].

In this experiment, separately, the spent adsorbents were transferred to a flask containing 100 mL of desorbing agent, 0.1 N HCl and soaked for overnight. After that, the adsorbents were filtered, washed thoroughly with distilled water, dried at 105 °C and then re-used as adsorbents for the adsorption of  $Pb^{2+}/Cd^{2+}$  ions. This procedure was repeated by four consecutive adsorption–desorption cycles. Results are presented in Fig. 11.

The results revealed that the removal capacity of the adsorbents was decreased with increasing number of regenerated cycles. Substantial removal efficiency was observed even after fourth regenerated cycle. This indicates that these adsorbents are stable and cost-effective.

### 3.8 Applications

The concentrations of lead and cadmium ions present in the industrial waste water collected at Hyderabad, India, were calculated before and after treatment with the adsorbents synthesized in the present study, AHAC, 'AHAC + n(Zr-Ce-Sm)oxide' and 'AHAC + b(Zr-Ce-Sm) oxide-Fe.Ali' beads. The results pertaining to the removal efficiency of the developed adsorbents and their experimental conditions are presented in Table 6.

As it can be seen from the table, the developed methodologies with the synthesized adsorbents in the present study were successfully remove the toxic lead and cadmium ions from industrial effluents at the extraction conditions established in this investigation.

### 3.9 Comparison

The adsorption capacities, for lead and cadmium ions, of the synthesized adsorbents in the present study, AHAC, 'AHAC + n(Zr-Ce-Sm) oxide' and 'AHAC + n(Zr-Ce-Sm) oxide-Fe.Ali' beads were compared with other adsorbents reported in the literature. These previous reports are related to the removal of either individual  $Pb^{2+}$  or  $Cd^{2+}$  ions from water but not both at a time. The present work reveals the simultaneous extraction of lead and cadmium ions at neutral or near neutral pHs. The results are presented in the Table 7.

The comparison of adsorption capacities of developed adsorbents with other adsorbents evidently confirmed that these adsorbents, AHAC, 'AHAC + n(Zr-Ce-Sm) oxide', 'AHAC + n(Zr-Ce-Sm) oxide-Fe.Ali' beads, could be considered as good sorbents for the removal of lead and cadmium ions from wastewater.

## 4 Conclusions

In this investigation, eco-friendly and cost-effective adsorbents based on active carbon and nano-mixed metal oxides are developed for the simultaneous removal of lead and cadmium ions from waste water. Active carbon derived from the stems of *Artocarpus heterophyllus* plant is identified to have affinity for lead and cadmium ions. The adsorption capacity is increased by doping the active carbon with nanometal (Zr-Ce-Sm) oxide synthesized by adopting new green routes. To prevent agglomeration, the composite of 'active carbon and mixed nanometal oxide' is embedded into iron-alginate

beads. Thus, the active carbon, AHAC, active carbon loaded with nanoparticles, 'AHAC + n(Zr-Ce-Sm) oxide' and iron alginate beads doped with their admixture, 'AHAC + n(Zr-Ce-Sm) oxide-Fe.Ali', are investigated as adsorbents. These adsorbents are characterized by various methods including XRD, FTIR, EDX and FESEM.

Different extractions conditions are investigated and optimized for the simultaneous removal of lead and cadmium ion and they are as follows: pH: 6.0, 6.5 and 7.0; adsorbent dosage: 1.0, 0.75 and 1.0 g/L and agitation time: 120, 60 and 90 min for AHAC, 'AHAC + n(Zr-Ce-Sm) oxide' and 'AHAC + n(Zr-Ce-Sm) oxide-Fe.Ali' beads respectively. The effect of co-ions on the simultaneous extraction is also investigated.

The experimental data for the simultaneous adsorption process of  $Pb^{2+}$  and  $Cd^{2+}$  ions is well analysed by various adsorption isotherms and kinetic models. Thermodynamic parameters are also explored to explain the mechanism of the adsorption process. Based on thermodynamic study and FTIR investigations, the mechanism of adsorption process involves the formation of a surface complex and/or ion-exchange between  $Pb^{2+}/Cd^{2+}$  with the surface functional groups of adsorbents. The maximum adsorption capacities of AHAC, 'AHAC + n(Zr-Ce-Sm) oxide' and 'AHAC + n(Zr-Ce-Sm)oxide-Fe.Ali' beads for  $Pb^{2+}$  and  $Cd^{2+}$  ions respectively are as follows: 15.0 and 20.0 mg/g; 28.0 and 32.6 mg/g; 34.0 and 44.3 mg/g. The spent adsorbents are regenerated with the eluent 0.1 N HCl and can be reused.

The adsorbents developed are efficient and convenient at neutral or nearly neutral pHs for the simultaneous removal of lead and cadmium ions. These adsorbents are successfully applied to treat real waste water samples of industries.

**Supplementary Information** The online version contains supplementary material available at <https://doi.org/10.1007/s13399-022-03063-2>.

**Acknowledgements** The authors thank the authorities of K.L.E.F. for providing the necessary facilities for this research work.

**Author contributions** KR: concept formation and guidance during the progress of this research work. SLP and SM: research scholars, collection of bio-materials for identifying the material having affinity for toxic lead and cadmium ions, optimization of extraction conditions, evaluation of results, evaluation of thermodynamic, kinetic and isothermal parameters to assess the mechanism of adsorption, application of the developed methodology for assessing the ability of bio-material to treat real polluted water.

## Declarations

**Conflict of interest** The authors declare no competing interests.

## References

1. Abdulrazak S, Hussaini K, Sani HM (2017) Evaluation of removal efficiency of heavy metals by low-cost activated carbon prepared from African palm fruit. *Appl Water Sci* 7(6):3151–3155. <https://doi.org/10.1007/s13201-016-0460>
2. Adamson AW, Gast AP (1997) *Physical Chemistry of Surfaces*, 6th Edition, Wiley, New York. <https://doi.org/10.1126/science.160.3824.179>.
3. Adeyanju CA, Ogunniyi S, Selvasembian R, Oniye MM, Ajala OJ, Adeniyi AG, Igwegbe CA, Ighalo JO (2022) Recent advances on the aqueous phase adsorption of carbamazepine. *Chem Bio Eng Reviews*. <https://doi.org/10.1002/cben.202100042>
4. Aharoni C, Ungarish M (1977) Kinetics of activated chemisorption. Part 2. Theoretical models. *J Chem Soc, Faraday Trans 1: Phys Chemi Condensed Phases* 73:456–464. <https://doi.org/10.1039/F19777300456>
5. Alslaibi TM, Abustan I, Ahmad MA, Abu Foul A (2015) Comparative studies on the olive stone activated carbon adsorption of  $Zn^{2+}$ ,  $Ni^{2+}$ , and  $Cd^{2+}$  from synthetic wastewater. *Desalination Water Treat* 3;54(1):166–77. <https://doi.org/10.1080/19443994.2013.876672>
6. Amarsingh Bhabu K, Theerthagiri J, Madhavan J, Balu T, Muralidharan G, Rajasekaran TR (2015) Cubic fluorite phase of samarium doped cerium oxide ( $CeO_2 \cdot 0.96Sm_{0.04}$ ) for solid oxide fuel cell electrolyte. *J Mater Sci Mater Electron* 27:1566–1573. <https://doi.org/10.1007/s10854-015-3925-z>
7. Amin MT, Alazba AA, Shafiq M (2021) Comparative removal of lead and nickel ions onto nanofibrous sheet of activated polyacrylonitrile in batch adsorption and application of conventional kinetic and isotherm models. *Membranes* 11(1):10. <https://doi.org/10.3390/membranes11010010>
8. Amina R, Abdelkader K, Mehdi A, Zoubida T, Djamilia I, Safia T, Andre D (2020) Lead and cadmium removal by adsorption process using hydroxyapatite porous materials. *Water Practice Technol* 15(1). <https://doi.org/10.2166/wpt.2020.003>
9. APHA (1998) *Standard methods for the examination of water and waste water*. APHA, Washington, DC
10. ASTM D4607–94 (2006) Standard test method for determination of iodine number of activated carbons. In *American Society for Testing and Materials*, pp 1–5
11. Badessa TS, Wakuma E, Yimer AM (2020) Bio-sorption for effective removal of chromium(VI) from wastewater using *Moringa stenopetala* seed powder (MSSP) and banana peel powder (BPP). *BMC Chemistry* 14(1):1–2. <https://doi.org/10.1186/s13065-020-00724-z>
12. Biftu WK, Suneetha M, Ravindhranath K (2020) De-fluoridation of polluted water using aluminium alginate beads doped with green synthesized 'nano  $SiO_2$  + nano  $CeO_2$ -ZrO<sub>2</sub>', as an effective adsorbent. *Chemistry Select* 5(47):15061–15074. <https://doi.org/10.1002/slct.202003744>
13. Biftu WK, Suneetha M, Ravindhranath K (2021) Sequential adsorptive removal of phosphate, nitrate and chromate from polluted water using active carbon derived from stems of *Carissa carandas* plant. *Water Practice Technol* 16(1):117–134. <https://doi.org/10.2166/wpt.2020.102> (IWA Publishing)
14. Biftu WK, Suneetha M, Ravindhranath K (2021b) Zirconium-alginate beads doped with H<sub>2</sub>SO<sub>4</sub>-activated carbon derived from leaves of *Magnoliaceae* plant as an effective adsorbent for the removal of chromate. *Biomass Convers Biorefin*. 1–16. <https://doi.org/10.1007/s13399-021-01568-w>
15. Brunauer S, Emmett PH, Teller E (1938) Adsorption of gases in multimolecular layers. *J Am Chem Soc* 60(2):309–19. <https://doi.org/10.1021/ja01269a023>

16. Bureau of Indian Standards (1989) Granular: methods of sampling and tests, New Delhi, India ISI, p. 877
17. Chien SH, Clayton WR (1980) Application of the Elovitch equation to the kinetics of phosphorus release and sorption in soils. *Soil Sci Soc Am J* 44:265–268
18. Coates, J. (2000) 'Interpretation of infrared spectra, a practical approach', in Meyer, R.A. (Ed.): *Encyclopedia of Analytical Chemistry*, pp.490–517, Wiley, Chicester.
19. Devi PV, Suneetha M, Ravindhranath K (2019) Effective activated carbon as adsorbent for the removal of copper (II) ions from wastewater. *Asian J Chem* 31(10):2233–2239
20. Dorofeev GA, Streletskii AN, Povstugar IV, Protasov AV, Elskov EP (2012) Determination of nanoparticle sizes by X-ray diffraction. *Colloid J* 74(6):675–685. <https://doi.org/10.1134/S1061933X12060051>
21. Dubinin MM (1947) The equation of the characteristic curve of activated charcoal. *InDokl Akad Nauk SSSR* 55:327–329
22. El-Hendawy AN, Samra SE, Girgis BS (2001) Adsorption characteristics of activated carbons obtained from corncobs. *Colloids Surf A* 180(3):209–221. [https://doi.org/10.1016/S0927-7757\(00\)00682-8](https://doi.org/10.1016/S0927-7757(00)00682-8)
23. Farooq A, Elsayed F, Naveed A (2014) Removal of lead from wastewater by adsorption using Saudi Arabian clay. *Int J Chem Environ Eng* 5(2):65–68
24. Francisco JA, Lorena A, Irene G, Felix AL (2018) Removal of Pb<sup>2+</sup> in Wastewater via adsorption onto an activated carbon produced from winemaking waste. *Metals* 8:697. <https://doi.org/10.3390/met8090697>
25. Freundlich HM (1906) Over the adsorption in solution. *J Phys Chem* 57(385471):1100–1107
26. Gao W, Wang Y, Basavanagoud B, Jamil MK (2017) Characteristics studies of molecular structures in drugs. *Saudi Pharm J* 25(4):580–6. <https://doi.org/10.1016/j.jsps.2017.04.027>
27. Hall KR, Eagleton LC, Acrivos A, Vermeulen T (1966) Pore-and solid-diffusion kinetics in fixed-bed adsorption under constant-pattern conditions. *Ind Eng Chem Fundam* 5(2):212–23. <https://doi.org/10.1021/i160018a011>
28. Ho YS, McKay G (1999) Pseudo-second order model for sorption processes. *Process Biochem* 34(5):451–465. <https://doi.org/10.1007/s11356-019-05050>
29. Igwegbe CA, Onukwuli OD, Ighalo JO, Okoye PU (2020) Adsorption of cationic dyes on *Dacryodes edulis* seeds activated carbon modified using phosphoric acid and sodium chloride. *Environ Processes*. <https://doi.org/10.1007/s40710-020-00467-y>
30. Igwegbe CA, Ighalo JO, Ghosh S, Ahmadi S, Ugonabo VI (2021) Pistachio (*Pistacia vera*) waste as adsorbent for wastewater treatment: a review. *Biomass Convers Biorefin*. <https://doi.org/10.1007/s13399-021-01739-9>
31. Jafari Kang A, Baghdadi M, Pardakhti A (2016) Removal of cadmium and lead from aqueous solutions by magnetic acid-treated activated carbon nanocomposite. *Desalin Water Treat* 57(40):18782–98. <https://doi.org/10.1080/19443994.2015.1095123>
32. Jellali S, Azzaz AA, Jeguirim M, Hamdi H, Mlayah A (2021) Use of lignite as a low-cost material for cadmium and copper removal from aqueous solutions: assessment of adsorption characteristics and exploration of involved mechanisms. *Water* 13:164. <https://doi.org/10.3390/w13020164>
33. Kishore Babu D, Ravindhranath K, Suneetha M (2021) Simple effective new bio-adsorbents for the removal of highly toxic nitrite ions from waste water. *Biomass Convers Biorefin*. <https://doi.org/10.1007/s13399-021-01677-6>
34. Lagergren S (1898) About the theory of so-called adsorption of soluble substances. *Kungliga Svenska, Vetenskapsakademiens, Handlingar*, 24(4), 1-39
35. Langmuir I (1918) The adsorption of gases on plane surfaces of glass, mica and platinum. *J Am Chem Soc* 40(9):1361–403. <https://doi.org/10.1021/ja02242a004>
36. Lata S, Singh PK, Samadder SR (2015) Regeneration of adsorbents and recovery of heavy metals: a review. *Int J Environ Sci Technol* 12:1461–1478. <https://doi.org/10.1007/s13762-014-0714-9>
37. Li B, Zhou F, Huang K, Wang Y, Mei S, Zhou Y, Jing T (2016) Highly efficient removal of lead and cadmium during wastewater irrigation using a polyethylenimine-grafted gelatin sponge. *Sci Rep* 6:33573. <https://doi.org/10.1038/srep33573>
38. Maryam A, Davood H, Somayyeh H, Vahideh K (2021) The nano-magnetite-loaded 2-mercaptobenzoxazole as an adsorbent for the selective removal of the Pb<sup>2+</sup>, Ni<sup>2+</sup> and Cd<sup>2+</sup> ions from aqueous solutions. *Korean J Chem Eng* 38(7):1510–1521. <https://doi.org/10.1007/s11814-021-0792-6>
39. Mekonnen DT, Alemayehu E, Lennartz B (2021) Adsorptive removal of phosphate from aqueous solutions using low-cost volcanic rocks: kinetics and equilibrium approaches. *Materials* 14:1312. <https://doi.org/10.3390/ma14051312>
40. Momina M, Mohammad S, Suzylawati I (2018) Regeneration performance of clay-based adsorbents for the removal of industrial dyes: a review. *RSC Adv* 8:24571–24587. <https://doi.org/10.1039/c8ra04290j>
41. Mukherjee S, Kumari D, Joshi M, An AK, Kumar M (2020) Low-cost bio-based sustainable removal of lead and cadmium using a polyphenolic bioactive Indian curry leaf (*Murrayakoengii*) powder. *Int J Hyg Environ Health* 226:113471. <https://doi.org/10.1016/j.ijheh.2020.113471>
42. Mukul CAC, Abdellaoui Y, Abatal M, Vargas J, Santiago AA, Barron-Zambrano JA (2019) Eco-efficient biosorbent based on *Leucaena leucocephala* residues for the simultaneous removal of Pb(II) and Cd(II) ions from water system: sorption and mechanism. *Bioinorg Chem Appl*. 1–13. <https://doi.org/10.1155/2019/2814047>
43. Naeema HY (2014) Removal of lead (II) from waste water by adsorption. *Int J Curr Microbiol App Sci* 3(4):207–228
44. Namasivayam C, Kadirvelu K (1997) Activated carbons prepared from coir pith by physical and chemical activation methods. *Bioresour Technol* 62(3):123–7. [https://doi.org/10.1016/S0960-8524\(97\)00074-6](https://doi.org/10.1016/S0960-8524(97)00074-6)
45. Onyango MS, Kojima Y, Aoyi O, Bernardo EC, Matsuda H (2004) Adsorption equilibrium modeling and solution chemistry dependence of fluoride removal from water by trivalent-cation-exchanged zeolite F-9. *J Colloid Interface Sci* 279(2):341–50. <https://doi.org/10.1016/j.jcis.2004.06.038>
46. Pentari D, Vamvouka D (2019) Cadmium removal from aqueous solutions using nano-iron doped lignite. *IOP Conf Ser Earth Environ Sci* 221:012135
47. Reddy JB, Sneha Latha P, Biftu WK, Suneetha M, Ravindhranath K (2021) Effective removal of Cu<sup>2+</sup> ions from polluted water using new bio-adsorbents. *Water Practice Technol* 16(2):566–581. <https://doi.org/10.2166/wpt.2021.019> (IWA Publishing)
48. Renu, MA, Singh K (2016) Heavy metal removal from wastewater using various adsorbents: A review. *J Water Reuse Desalination* 7(4):387–419. <https://doi.org/10.2166/WRD.2016.104>
49. Singanan M (2011) Removal of lead (II) and cadmium (II) ions from wastewater using activated biocarbon. *ScienceAsia* 37:115–119. <https://doi.org/10.2306/scienceasia1513-1874.2011.37.115>
50. Sneha Latha P, Biftu WK, Suneetha M, Ravindhranath K (2022) Adsorptive removal of toxic chromate and phosphate ions from polluted water using green synthesized nano metal (Mn-Al-Fe) oxide. *Biomass Convers Biorefin*. <https://doi.org/10.1007/s13399-021-02293-0>
51. Sneha Latha P, Biftu WK, Suneetha M, Ravindhranath K (2021a) Simultaneous removal of Lead and cadmium ions

- from simulant and industrial waste water: using *Calophyllum* plant materials as sorbents. *Int J Phytoremediation* 1–15. <https://doi.org/10.1080/15226514.2021.1961121>
52. SnehaLatha P, Biftu WK, Suneetha M, Ravindhranath K (2021b) De-fluoridation studies: using Lanthanum-alginate-beads impregnated with green synthesized nSiO<sub>2</sub> and active carbon of *Terminalia Ivorensis* plant as an effective adsorbent. *Int J Environ Sci Technol*. <https://doi.org/10.1007/s13762-021-03575-w>
53. SnehaLatha P, Biftu WK, Suneetha M, Ravindhranath K (2021c) Effective adsorbents based on nano mixed (Al-Fe-Zr) oxide synthesised by new green methods: for the simultaneous extraction of phosphate and chromate from contaminated water. *Int J Environ Anal Chem*. <https://doi.org/10.1080/03067319.2021.1927004>
54. Sujitha R, Ravindhranath K (2018) Removal of lead (II) from wastewater using active carbon of *Caryota urens* seeds and its embedded calcium alginate beads as adsorbents. *J Environ Chem Eng* 6(4):4298–4309. <https://doi.org/10.1016/j.jece.2018.06.033>
55. Sun H, He X, Wang Y, Cannon FS, Wen H, Li X (2018) Nitric acid-anionic surfactant modified activated carbon to enhance cadmium(II) removal from wastewater: preparation conditions and physicochemical properties. *Water Sci Technol* 78:1489–1498
56. Suneetha M, Ravindhranath K (2018) Removal of Nitrites from polluted waters using adsorbents derived from *Phyllanthus neruri* plant. *Indian J Chem Technol* 25:345–352
57. Suneetha M, Ravindhranath K (2017) Adsorption of Nitrite ions from wastewater using bio-sorbents derived from *Azadirachta indica* plant. *Asian J Water Environ Pollut* 14(2):71–79. <https://doi.org/10.3233/AJW-170017>
58. Suneetha M, Syama Sundar B, Ravindhranath K (2015a) Removal of fluoride from polluted waters using active carbon derived from barks of *Vitex negundo* plant. *J Anal Sci Technol*, 6(15). <https://doi.org/10.1186/s40543-014-0042-1>
59. Suneetha M, SyamaSundar B, Ravindhranath K (2015b) De-fluoridation of waters using low-cost HNO<sub>3</sub> activated carbon derived from stems of *Senna occidentalis* plant. *Int J Environ Technol Manage* 18(5/6):420–447. <https://doi.org/10.1504/IJETM.2015.073079>
60. Suneetha M, SyamaSundar B, Ravindhranath K (2015c) Extraction of fluoride from polluted waters using low-cost active carbon derived from stems of *Acalypha indica* plant. *Asian J Water Environ Pollut* 12(3):33–49. <https://doi.org/10.3233/AJW-150005>
61. Sunil K, Jayant K (2014) Regeneration and recovery in adsorption- a review. *Int J Innov Sci Eng Technol* 1(8):61–64
62. Temkin MJ, Pyzhev V (1940) Recent modifications to Langmuir isotherms. *Acta Physiochim USSR* 12:217–222
63. Thabede PM, Shooto ND, Naidoo EB (2020) Removal of methylene blue dye and lead ions from aqueous solution using activated carbon from black cumin seeds. *S Afr J Chem Eng* 33:39–50. <https://doi.org/10.1016/j.sajce.2020.04.002>
64. World Health Organization (2011a) Lead in drinking water. Report No. WHO/SDE/WSH/03.04/09/ Rev/1, Geneva
65. World Health Organization (2011b) Cadmium in drinking water. Report No. WHO/SDE/WSH/03.04/80/ Rev/1, Geneva

**Publisher's note** Springer Nature remains neutral with regard to jurisdictional claims in published maps and institutional affiliations.